

# Plasma stratification in AC discharges in noble gases at low currents

Vladimir I. Kolobov<sup>1,2</sup> and Robert R. Arslanbekov<sup>2</sup>

<sup>1</sup>*University of Alabama in Huntsville, Huntsville, AL, USA*

<sup>2</sup>*CFD Research Corporation, Huntsville, AL, USA*

## Abstract

A hybrid kinetic-fluid model is used to study plasma stratification in alternating current (AC) discharges in noble gases at low plasma densities. Self-consistent coupled solutions of a non-local kinetic equation for electrons, a drift-diffusion equation of ions, and a Poisson equation for the electric field are obtained for a positive column with periodic boundary conditions and for the entire discharge to study near-electrode effects within a 1d model with radial ambipolar loss. A simplified two-level excitation-ionization model neglects the nonlinear effects due to stepwise ionization, gas heating, and Coulomb interactions among electrons. Standing striations are obtained for the reduced values of electric fields,  $E/p$ , corresponding to the inelastic energy balance of electrons in a range of driving frequencies. An analog of Novak's law,  $\Lambda = \varepsilon_1/(e\langle E \rangle)$  (striation length proportional to the excitation threshold of atoms and inversely proportional to the mean square root of the electric field  $\langle E \rangle$ ), is observed in simulations, indicating the nonlocal nature of standing striations in AC discharges at low plasma densities. Stratified plasma operates in a dynamic regime for a wide range of driving frequencies because heat conduction occurs much faster than the ambipolar diffusion controlled by slow ion motion. We demonstrate that standing striations in symmetric AC discharges previously observed in experiments are similar to moving striations in DC discharges and are both due to nonlocal kinetic effects at low discharge currents.

## I. Introduction

Plasma stratification into bright and dark layers along electric current has been commonly observed in discharges of noble gases. In DC discharges, striations usually move at high speeds and are not visible to the naked eye [1]. Standing striations have been observed in symmetric AC discharges; they move slowly in the presence of an asymmetry or a small DC component of the electric field. Striations have been experimentally observed in capacitively coupled plasma (ICP), inductively coupled plasma (ICP), and dielectric barrier discharges (DBD) at various gas pressures and driving frequencies. A similar nature of moving striations in DC discharges and standing striations in high-frequency AC discharges has been demonstrated by Nedospasov [2,3] using linear analysis of a dispersion equation for strata in noble gases. However, plasma stratification remains a subject of active research, and several recent studies in atomic [4,5,6,7] and molecular [8,9] gases have been published.

There are two mechanisms of plasma stratification in noble gases at low gas pressures. One is associated with the nonlinearity of the ionization rate to electron density, and the other is due to non-local electron kinetics. An intrinsic length  $\lambda_\varepsilon = \varepsilon_1/(eE)$  defines the characteristic striation length in the latter case. Over this length, an electron gains kinetic energy equal to the excitation threshold of atoms  $\varepsilon_1$  in the electric field  $E$  ( $e$  is the electron charge). Kinetic resonances at the

wavelengths  $\Lambda \approx \lambda_e$  and its integer fractions, and various moving striations have been observed in DC discharges in noble gases [10]. The present paper shows that this intrinsic length also defines the length of standing striations in symmetric AC discharges at low currents.

Despite several previous publications, the origin of AC plasma stratification has remained unclear. Timofeev [11] first described a “thermocurrent” instability that could lead to stratification of DC and AC discharges. The instability occurs when the thermo-diffusion electron flux is directed opposite to the diffusion flux and exceeds its magnitude. The review [12] and references cited therein explain that the maximal increment of this instability is observed for short wavelengths (compared to the electron energy relaxation length). Without Coulomb collisions, the fluid description of electrons under such conditions is inaccurate. Therefore, a kinetic model using a Particle-in-Cell (PIC) method [13] or a solution of a non-local kinetic equation [14] should be used under these conditions. Standing striations in CCP obtained with a hybrid model to be described in the present paper have been briefly reported [15], but no details have been provided.

Several publications have experimentally observed the stratification of AC discharges in noble gases [16,17]. The fluid model [18] successfully explained the stratification at high plasma densities when Coulomb collisions among electrons are essential. This model was recently used to analyze ICP stratification [5, 6]. In the present paper, a hybrid kinetic-fluid model previously used for moving striations in DC discharges at low plasma densities [19] is adapted to simulations of standing striations in AC discharges. The model uses a Fokker-Planck kinetic solver for electrons and a fluid model for ions with simple two-level excitation-ionization kinetics. With such a simplified 1D model, we do not aim for a detailed comparison with the experiment. Our goal is to clarify the essence of the phenomena and to illustrate the peculiarities of electron kinetics in phase space, which takes place in stratified plasma of noble gases.

We show that stratified plasma operates in a dynamic regime for a wide range of driving frequencies. In the dynamic regime, the plasma density oscillates weakly during the AC period, but the electron energy probability function (EEPF), the electron mean energy (temperature), and electron-induced excitation and ionization rates oscillate substantially in time during the AC period. The dynamic regime was previously analyzed for low-frequency ICP [20] and a striation-free AC positive column [21]. This regime becomes possible because free electron diffusion occurs much faster than the ambipolar diffusion controlled by slow ion motion. In spatially inhomogeneous plasmas, electrons with different energies diffuse in phase space much faster than an average electron within the ambipolar diffusion model. Therefore, spatial and temporal non-locality correlate in stratified plasma of AC discharges in noble gases.

In the present paper, we consider the case of low ionization degree (plasma density) when the nonlinear processes associated with stepwise ionization, Coulomb collisions among electrons, and gas heating are insignificant. The paper's plan is as follows: We first briefly describe the computational model and boundary conditions. The central part analyzes plasma stratification in a positive column of AC discharges in Argon and Neon with periodic boundary conditions. We briefly describe the impact of near-electrode effects on CCP stratification. Finally, we identify open questions and plans for future research.

## II. Computational model

The hybrid model used in the present paper was first described in [22] and later adapted in [19] to study striations in DC discharges and the radial structure of positive columns in AC discharges [21]. This model is extended to analyze plasma stratification in AC discharges in noble gases.

### 1. Electron kinetics

Using two-term spherical harmonics expansion, the Boltzmann kinetic equation for electrons in weakly ionized collisional plasma can be reduced to a set of two coupled equations [23]:

$$\frac{\partial f_0}{\partial t} + \frac{v}{3} \nabla \cdot \mathbf{f}_1 - \frac{1}{3v^2} \frac{\partial}{\partial v} \left( v^2 \frac{e\mathbf{E}}{m} \cdot \mathbf{f}_1 \right) = S_0 \quad (1)$$

$$\frac{\partial \mathbf{f}_1}{\partial t} + v \mathbf{f}_1 = -v \nabla f_0 + \frac{e\mathbf{E}}{m} \frac{\partial f_0}{\partial v} \quad (2)$$

Here,  $e$  and  $m$  are the unsigned electron charge and mass,  $\mathbf{E}$  is the electric field vector,  $\nu(v)$  is the transport collision frequency and  $S_0$  describes energy exchange in elastic and inelastic electron-atom collisions, electron-electron interactions, and ionization-recombination processes.

Equation (1) expresses the divergence of a flux ( $\Phi$ ,  $\Gamma$ ) in a 4D phase space ( $\mathbf{r}$ ,  $u$ ):

$$\frac{\partial f_0}{\partial t} + \nabla \cdot \Phi - \frac{1}{v} \frac{\partial}{\partial u} (v\Gamma) = S_0, \quad (3)$$

where  $u = mv^2/(2e)$  is the volt-equivalent of the electron kinetic energy and

$$\Phi = \frac{v}{3} \mathbf{f}_1, \quad \Gamma = \mathbf{E} \cdot \Phi \quad (4)$$

The speed  $v$  plays the role of the Lamé coefficient. Equation (2) shows that  $\mathbf{f}_1$  depends on the local value of the electric field, i.e. the two-term approximation results in Ohm's law [24].

The general solution of Eq. (2) can be written in the form [25]:

$$\mathbf{f}_1(\mathbf{r}, v, t) = -ve^{-vt} \int_{-\infty}^t e^{vt'} \left[ \nabla f_0 - \frac{e\mathbf{E}(\mathbf{r}, t')}{mv} \frac{\partial f_0}{\partial v} \right] dt' \quad (5)$$

The main contribution to integral (5) comes from a small vicinity of the point  $t$  about the size  $\sim \nu^{-1}$ . As the characteristic time scale of the time-variation  $f_0$  is larger than  $\nu^{-1}$ , the derivatives can be removed from the integral sign in (5) to obtain:

$$\mathbf{f}_1(\mathbf{r}, v, t) = -\frac{v}{v} \left[ \nabla f_0 - \mathcal{E}(t) \frac{\partial f_0}{\partial v} \right] \quad (6)$$

Here, we introduced an effective field:

$$\mathcal{E}(\mathbf{r}, t) = e^{-\nu t} \int_{-\infty}^{\nu t} e^{\tau} \mathbf{E}(\mathbf{r}, \tau) d\tau \quad , \quad (7)$$

which accounts for temporal dispersion. Using (6), the spatial flux becomes

$$\Phi = -D_r \left( \nabla f_0 - \mathcal{E} \frac{\partial f_0}{\partial u} \right) \quad (8)$$

where  $D_r = v^2/(3\nu)$  is the spatial diffusion coefficient in phase space. Substituting (4) into (1), we obtain a Fokker-Planck (FP) kinetic equation for  $f_0(\mathbf{r}, u, t)$  in a 4D phase space  $(\mathbf{r}, u)$ :

$$\frac{\partial f_0}{\partial t} - \left( \nabla - \mathbf{E} \frac{1}{\sqrt{u}} \frac{\partial}{\partial u} \sqrt{u} \right) \cdot D_r \left( \nabla - \mathcal{E} \frac{\partial}{\partial u} \right) f_0 = S_0 \quad , \quad (9)$$

which can be rewritten in the form:

$$\frac{\partial f_0}{\partial t} - \nabla_4 \cdot (\mathbf{D} \nabla_4 f_0) = S_0 \quad , \quad (10)$$

where  $\nabla_4$  denote the divergence and grad operators in the 4D phase space and  $\mathbf{D}$  a diffusion tensor:

$$\mathbf{D} = D_r \begin{pmatrix} \mathbf{I}_3 & -\mathcal{E} \\ -\mathbf{E} & \mathcal{E} \cdot \mathbf{E} \end{pmatrix} . \quad (11)$$

Here  $\mathbf{I}_3$  denotes the unit tensor in 3D configuration space. The kinetic equation (10) has already been used (in 2D phase space) to analyze the axial and radial structure of DC discharges and plasma stratification [14, 19, 21]. It also appeared in the study of fully ionized plasma [26].

The most favorable conditions for plasma stratification are observed when the two terms in the brackets of (9) are of the same order, which corresponds to a spatial scale  $\Lambda = u/E$ . In this case, electron fluxes in configuration space and energy described by the left part of Eq. (10) are of the same order. The time scale for  $f_0(\mathbf{r}, u, t)$  variation is defined by a characteristic frequency  $\nu_E = (E/u)^2 D_r$  due to electron diffusion in phase space and the frequency,  $\nu_0 = S_0/f_0$ , which controls energy flow in collisions and electron generation processes. For slow variations of  $E(t)$  compared to  $\max\{1/\nu_E, 1/\nu_0\}$ , the time derivative in (9,10) can be neglected and  $f_0(t)$  depends on the instantaneous value of the electric field. For fast variations of  $E(t)$ ,  $f_0$  depends on the average value of the electric field.

The right-hand side of Eqs. (9, 10) describes the particle and energy flux due to collisions and electron generation processes. The electron energy loss in quasi-elastic collisions is described by:

$$C_{el} = \frac{1}{\sqrt{u}} \frac{\partial}{\partial u} \left( u^{3/2} \delta \nu f_0 \right) \quad (12)$$

where  $\delta$  is the fraction of electron energy lost in quasi-elastic collisions. The excitation of an atomic state with the energy threshold  $\varepsilon_1$  is described by

$$C_{ex} = -\nu^*(u)f_0(u) + \frac{\sqrt{u+\varepsilon_1}}{\sqrt{u}}\nu^*(u + \varepsilon_1)f_0(u + \varepsilon_1) \quad (13)$$

where  $\nu^*(u)$  is the corresponding inelastic collision frequency. The operators (11) and (12) conserve the number of electrons. The total frequency of the EEDF relaxation in collisions is  $\nu_u(u) = \delta\nu + \nu^*(u)$ . For noble gases,  $\nu_u(u)$  is a strong function of energy. At low energies,  $u < \varepsilon_1$ ,  $\nu_u(u) = \delta\nu \ll \nu$ , where  $\delta = 2m/M \ll 1$ . At energies  $u > \varepsilon_1$ ,  $\nu_u(u) \approx \nu^*(u)$ , and frequency of inelastic collisions  $\nu^*(u) \leq \nu(u)$ . For molecular gases,  $\delta$  could be about the unity due to the excitation of rotational and vibrational states of molecules and  $\nu_u = \delta\nu \approx \nu$  in the corresponding energy range.

The direct ionization by electron impact is described as:

$$C_{ion} = -\nu^{ion}(u)f_0(u) + 4\frac{\sqrt{2u+\varepsilon_{ion}}}{\sqrt{u}}\nu^{ion}(2u + \varepsilon_{ion})f_0(2u + \varepsilon_{ion}) \quad (14)$$

where  $\nu^{ion}(u)$  is the ionization frequency and  $\varepsilon_{ion}$  is the ionization threshold. The operator (13) describes the generation of new electrons, assuming that the kinetic energy is evenly distributed between the primary and secondary electrons after an ionization event. The frequency of ionization is the slowest process, as the production of electron-ion pairs in ionization events must be balanced by their loss, which is controlled by slow ion transport processes. For this reason, details of the energy redistribution between the primary and secondary electrons are not particularly important. Using (13), it is easy to switch off the electron generation but still consider the inelastic energy loss with the quantum of  $\varepsilon_{ion}$ . We have used this feature to analyze the effect of secondary electron generation on plasma stratification.

## 2. Discharge model

Below, we assume that plasma is contained in a long cylindrical tube of radius  $R$  and is maintained by the axial electric field,  $E(x, t)$ . The charged particles are lost due to ambipolar diffusion and surface recombination at the wall. We rewrite the kinetic equation (10) for a 2D phase space  $(x, u)$  as:

$$\frac{\partial f_0}{\partial t} - \nabla \cdot (\mathbf{D}_2 \nabla f_0) = C_0 - C_{wall} \quad . \quad (15)$$

The diffusion tensor  $\mathbf{D}_2$  is defined as:

$$\mathbf{D}_2 = D_r \begin{pmatrix} 1 & -\mathcal{E} \\ -E & \mathcal{E}E \end{pmatrix}, \quad (16)$$

and the radial loss  $C_{wall} E(x, t)$  is added. The loss of electrons at the wall can be included in the form [27]:

$$C_{wall} = -\frac{1}{3} \left( \frac{v}{R} \right) f_0(u) \theta(u - \Phi_w) \quad (17)$$

where  $\Phi_w(x, t)$  is the wall potential relative to the axis and  $\theta(x)$  is the step function. This expression assumes that only fast electrons with kinetic energies exceeding  $\Phi_w$  can escape to the wall. However, the calculation of  $\Phi_w(x, t)$  may require two-dimensional analysis in configurational space  $(x, r)$ , and we plan to do that in future work.

In the present work, we used a simpler expression like in the DC discharges [19]:

$$C_{wall} = -f_0/\langle\tau_{wall}\rangle = -f_0\langle\nu_i\rangle \quad (18)$$

where  $\langle\nu_i\rangle$  is the space-averaged ionization frequency and  $\tau_{wall}$  is the time of electron diffusion to the wall. For AC discharges, the averaging operator  $\langle\dots\rangle$  also included the time-averaging over an AC cycle. This model assumes that all electrons are lost at an equal rate, equal to the average rate at which they are created over the striation length during the AC period. This model of average losses may be appropriate for  $\omega\langle\tau_{wall}\rangle < 1$ . Our tests showed that the choice of the electron loss model does not significantly affect the results for the reasons discussed above.

We introduce a computational grid in phase space for the numerical solution of the FP kinetic equation (11). The energy  $u_{max}$  is selected about 2-3  $\varepsilon_1$ . The typical number of cells in energy and space is 50 and 100. The boundary condition is specified as  $f_0(x, u = u_{max}) = 0$ . The boundary condition at  $u = 0$

$$\frac{\partial f_0}{\partial x} - E \frac{\partial f_0}{\partial u} \rightarrow 0 \quad (19)$$

ensures the absence of electron flux from the boundary at  $u = 0$ . The periodic boundary conditions in space for simulations of the positive column and the boundary conditions at electrodes for simulations of the entire discharge are discussed below.

Ions are described using a drift-diffusion model:

$$\frac{\partial n_i}{\partial t} + \frac{\partial}{\partial x} \left( \mu_i n_i E(x) - D_i \frac{\partial n_i}{\partial x} \right) = I - \frac{n_i}{\tau} \quad (20)$$

where  $\mu_i$  and  $D_i$  are the ion mobility and diffusion coefficients, and  $I$  is the ionization rate by electron impact. The ion loss term matches the electron loss,  $\langle\nu_i\rangle\tau = 1$ , where  $\langle\nu_i\rangle$  is the ionization frequency averaged over striation length. This condition ensures charge conservation over striation length. The electric field is calculated from the Poisson equation. We assume that the initial EEDF is Maxwellian, and the initial ion density equals the electron density.

The coupled set of the FP kinetic equation for electrons (1), the drift-diffusion for ions (12) and the Poisson equation for the electric field was solved using COMSOL with an implicit (BDF) time-stepping method. A direct (MUMPS) solver was employed at each time step for all quantities. We have not used the logarithmic transformation of the ion drift-diffusion and the FP kinetic equations used in our previous work [19]. We found that the convergence of the coupled equations with different dimensionality, solved simultaneously, is substantially better without this transformation

(particularly important for long transient simulations), and small negative values of  $f_0$  and  $n_i$  do not affect the results.

### 3. Periodic boundary conditions for positive column

The positive column is usually considered an autonomous system weakly influenced by near-electrode processes. Without striations, the positive column plasma is axially uniform with a local balance of the ionization and particle loss to the wall due to ambipolar diffusion or volume recombination. To analyze plasma stratification of the positive column, we apply periodic boundary conditions for the EEDF and the particle fluxes at the left and right boundaries:

$$\begin{aligned} (f_0)_{\text{left}} &= (f_0)_{\text{right}} \\ -(\mathbf{D}_2 \nabla f_0 \cdot \hat{n})_{\text{left}} &= (\mathbf{D}_2 \nabla f_0 \cdot \hat{n})_{\text{right}} \end{aligned}$$

where  $\hat{n}$  denotes the unit normal to the boundary. This BC ensures the continuity of the EEDF and the electron flux in phase space. We also apply periodic boundary conditions for ions by making the ion density and the ion flux equal at the boundaries:

$$\begin{aligned} (n_i)_{\text{left}} &= (n_i)_{\text{right}} \\ -\left( \left( \mu_i n_i E(x) - D_i \frac{\partial n_i}{\partial x} \right) \right)_{\text{left}} &= \left( \left( \mu_i n_i E(x) - D_i \frac{\partial n_i}{\partial x} \right) \right)_{\text{right}} \end{aligned}$$

Using periodic BCs for electrons and ions implies an integer number of waves fit the positive column. Also, such boundary conditions ensure that the total number of electrons and ions remains the same in the plasma (provided that matching electron and ion losses are used). As the total space charge remains zero (initially, a quasineutral plasma is assumed with  $n_e = n_i$ ) along the striation length, the periodic BC for the electric field  $E(\text{left}) = E(\text{right})$  is automatically satisfied. Therefore, we can prescribe the electric potential at the boundaries to specify the potential drop  $U$  over the length  $L$ .

The radius of the tube  $R$  was computed from:

$$R = 2.4 \sqrt{\frac{D_a}{\langle v_i \rangle}} \quad (21)$$

The averaged electron temperature  $\langle T_e \rangle$  was used to evaluate the ambipolar diffusion coefficient,  $D_a$  at  $\omega \langle \tau_{\text{wall}} \rangle < 1$ .

For the DC striations studied previously [19], the radius of the tube  $R$  was computed from:

$$R = 2.4 \sqrt{\frac{\langle D_a \rangle}{\langle v_i \rangle}} \quad (22)$$

where spatial averaging over the striation length is calculated as:

$$\langle f \rangle(t) = \frac{1}{\Lambda} \int_0^\Lambda dx' f(x', t) \quad (23)$$

This allowed the tube radius (not an input parameter but a computed quantity in this model) to become a spatially independent quantity at periodic convergence (periodic steady state). For AC striations in this paper, we have also added averaging over the AC period  $T$ :

$$\langle f \rangle = \frac{1}{\Lambda T} \int_{t-T}^t \int_0^\Lambda dt' dx' f(x', t') \quad (24)$$

This allowed the tube radius to become spatially- and time-independent at periodic convergence (e.g., frozen density but oscillating temperature regime). Due to current COMSOL limitations, “running” time averaging was used instead:

$$\langle f \rangle = \frac{1}{\Lambda t} \int_0^t \int_0^\Lambda dt' dx' f(x', t') \quad (25)$$

For computing the tube radius, oscillations of the electron temperature in the dynamic regime at  $\omega \langle \tau_u \rangle < 1$ , have been neglected.

### III. Standing striations in AC discharges

We obtained standing striations in the AC positive column with periodic BCs in Argon and Neon over a wide range of driving frequencies from 0.1 to 50 MHz. Our model resolved the AC period to compute the EEDF and the ion transport. We found that plasma density responds weakly to oscillating electric fields at driving frequencies at  $\omega \langle \tau_a \rangle > 1$ . On the other hand, at frequencies below ~25-50 MHz in Argon at  $p = 0.5$  Torr, the EEDF and electron mean energy oscillated over the AC period because  $\omega \langle \tau_u \rangle < 1$ . The length of standing striations of a few tube radii weakly depended on driving frequency. Higher frequencies required longer simulation times.

#### 1. Standing Striations in Argon

Figure 1 shows calculated spatial distributions of plasma properties in Argon at pressure  $p = 0.4$  Torr, driving frequency of 1 MHz, and voltage  $U = 55$  V. The column length is  $L = 6$  cm, and the electric field has amplitude  $E_0 = \frac{U}{L} = 9.17$  V/cm. Under these conditions, the calculated Debye length 0.07 cm is much smaller than the tube radius  $R = 0.37$  cm. Four standing striations with a length  $\Lambda = 1.5$  cm were formed in our simulations. The time-averaged electron and ion densities deviate slightly near their max and min values. Substantial spatial oscillations of the time-averaged electron temperature are observed. For most of the AC period, the electric field reverses direction in space, forming collisional double layers, typical of strongly nonlinear waves.

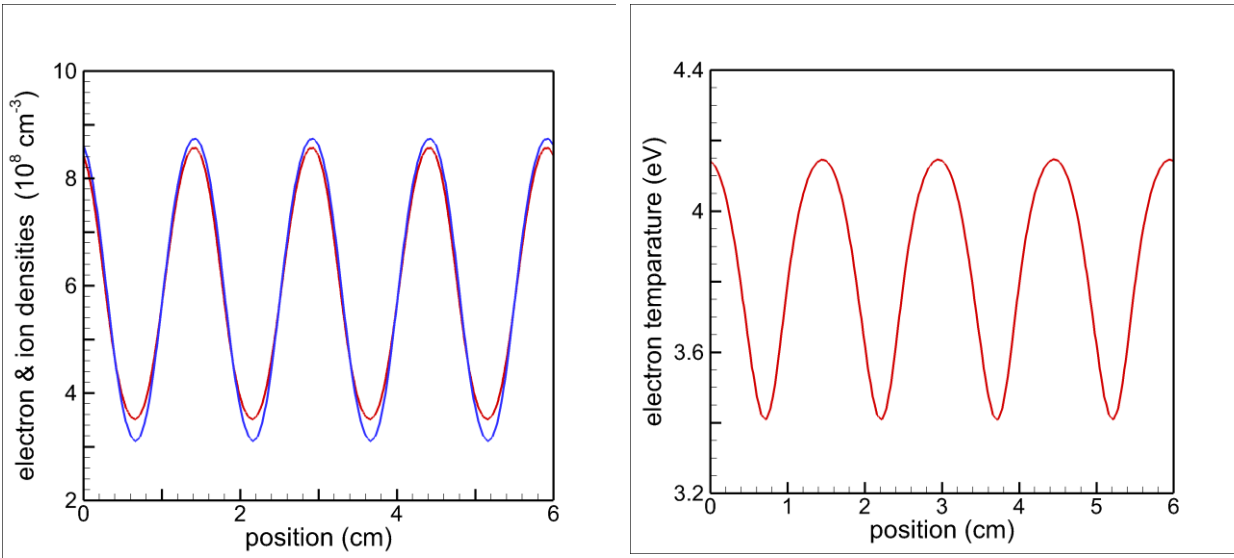
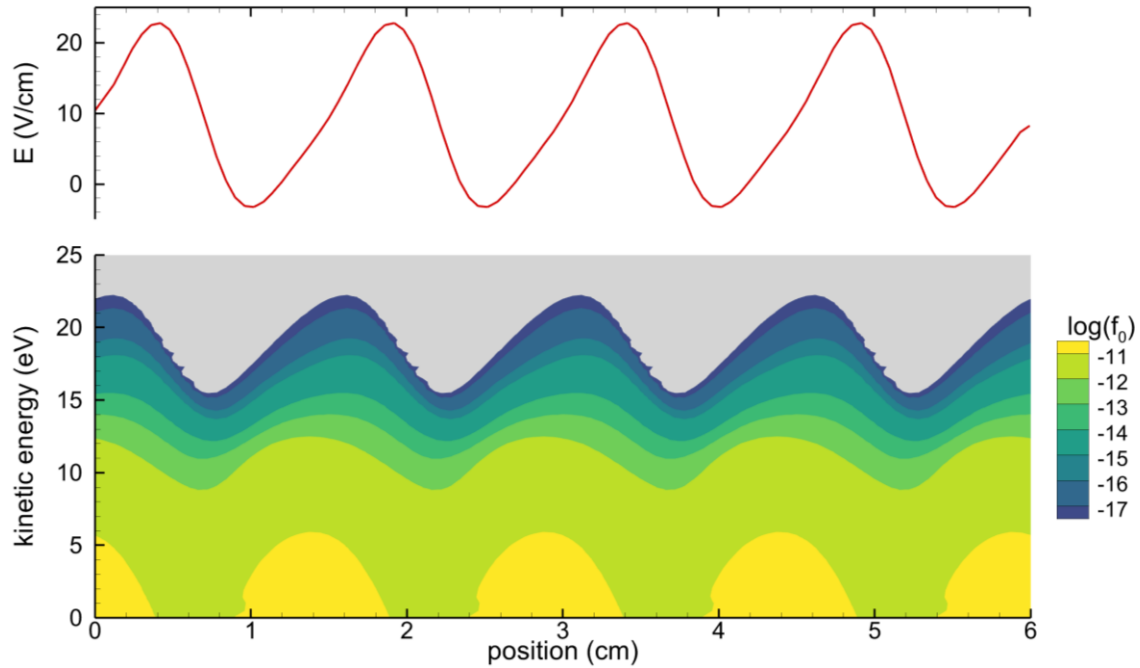


Figure 1: Instantaneous distribution of the electric field and EEDF contours (top) and time average electron and ion densities and electron temperature (bottom), Argon,  $p = 0.4$  Torr, 1 MHz,  $E_0 = 9.17$  V/cm.

By changing the driving frequency and applied voltage, we could change the wavelength and modulation depth of the striations. The amplitude of the electric field,  $E_0$ , has the most substantial effect. Figure 2 shows results for 0.4 Torr, 5 MHz, and  $U = 80$  V. These conditions correspond to  $E_0 = 13.3$  V/cm, the tube radius of  $R = 3.2$  mm, and Debye length of about 0.5 mm. The striation length is  $\Lambda = 1.6$  cm. As in the previous case of 1 MHz, the discharge operates in a dynamic regime. The ion and electron densities remain steady during the AC period, but the electron temperature and the ionization rate oscillate substantially around their average values. We refer

these conditions as a dynamic regime of discharge operation. The amplitude of modulations for these quantities decreases gradually with increasing driving frequency.

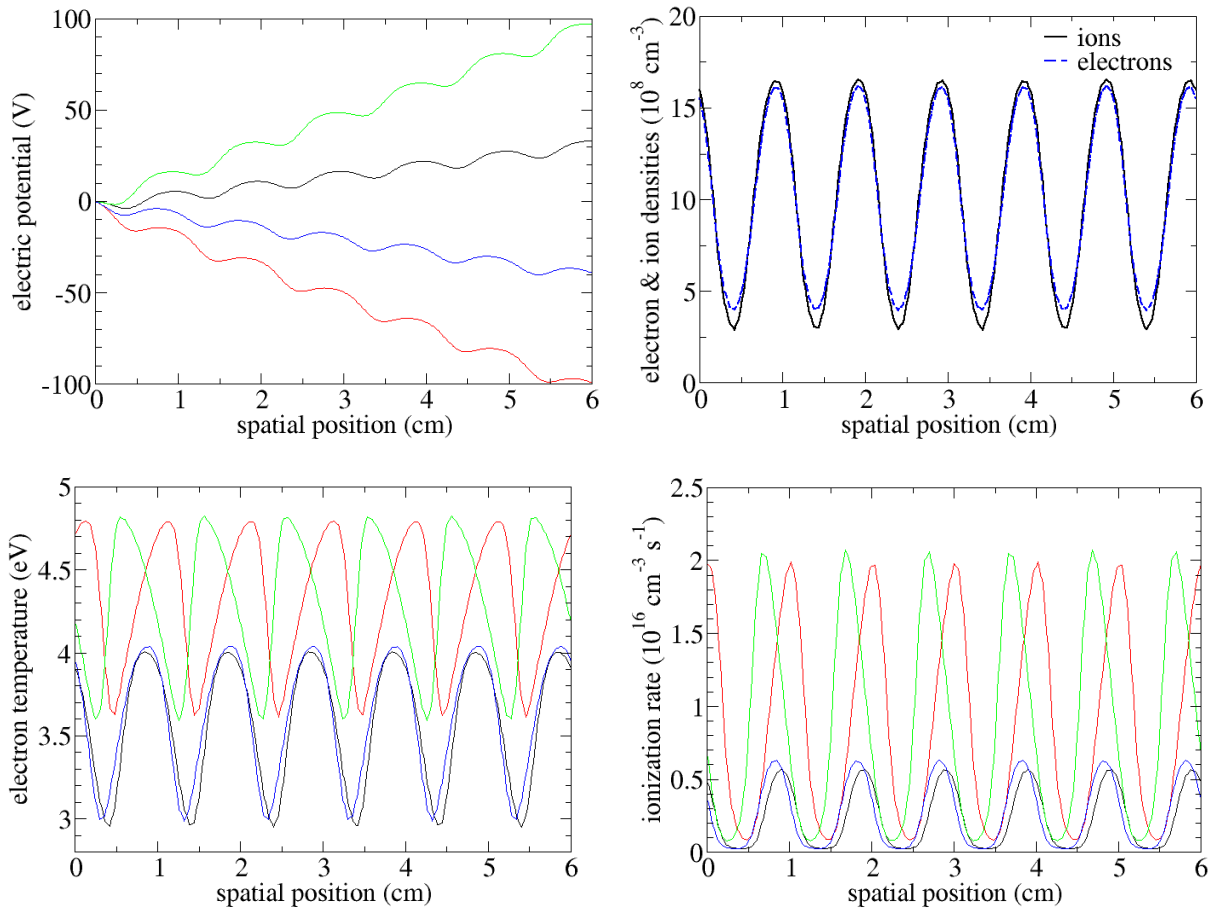


Figure 2: Spatial distributions of the electric potential, electron and ion densities, electron temperature, and the ionization rate at four times (color) during the AC period. Argon, 0.4 Torr, 5 MHz, and  $E_0 = 13.3$  V/cm.

Figure 3 shows an example of temporal variations of plasma properties in Argon at 0.4 Torr, at frequency 25 MHz,  $U = 100$  V,  $n = 10^{15}$  m<sup>-3</sup>,  $L = 3$  cm. This corresponds to the large electric field of amplitude  $E_0 = 33.3$  V/cm, small tube radius of  $R = 1$  mm, and Debye length of about 0.5 mm, comparable to the tube radius. The striation length is  $\Lambda = 6$  mm. Substantial differences in electron and ion densities occur at the positions of their maximum and minimum values. The time modulations of electron and ion densities are negligible. However, substantial modulations of electron temperature and the rates of electron-induced inelastic processes (at a double AC frequency like those shown in Figure 2) are observed. These modulations are associated with oscillations of the EEPF at low and high energies. The low-energy electrons control the heat transport processes and the electron temperature (mean energy) dynamics. The EEPF tail defines the rates of electron-induced inelastic processes.

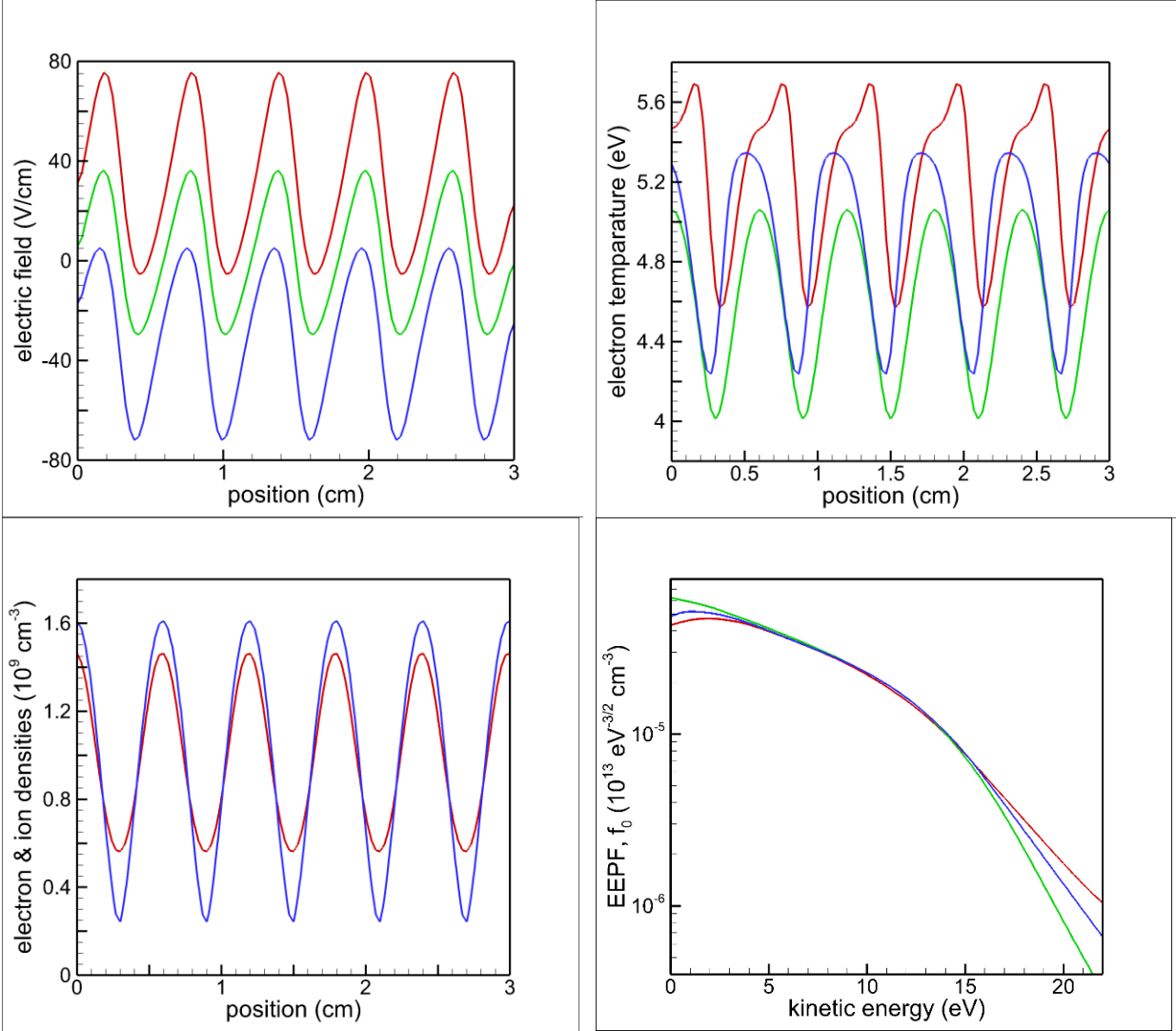


Figure 3: Instantaneous spatial distributions of the electric field, electron temperature, electron and ion densities, and EEDF at 6 mm for 25 MHz,  $E_0 = 33.3$  V/cm.

To better understand the effects of gas pressure and driving frequency, we show the results below for  $p = 0.1$  Torr and driving frequencies 0.1 and 50 MHz.

Figure 4 shows the results for 0.1 MHz and voltage  $U = 55$  V. The column length is  $L = 24$  cm, and the electric field amplitude is  $E_0 = 1.86$  V/cm. The calculated tube radius is  $R = 5$  cm, and the striation length is  $\Lambda = 8$  cm. For most of the AC period, the electric field does not change sign in space, indicating low-amplitude waves. Noticeable oscillations of the electron and ion densities over their average values are observed during the AC period. Strong oscillations of electron temperature in space and time are observed at this low driving frequency compared to the previous cases. This case is at the boundary of the applicability of our model, which assumes  $\omega\langle\tau_a\rangle > 1$ .

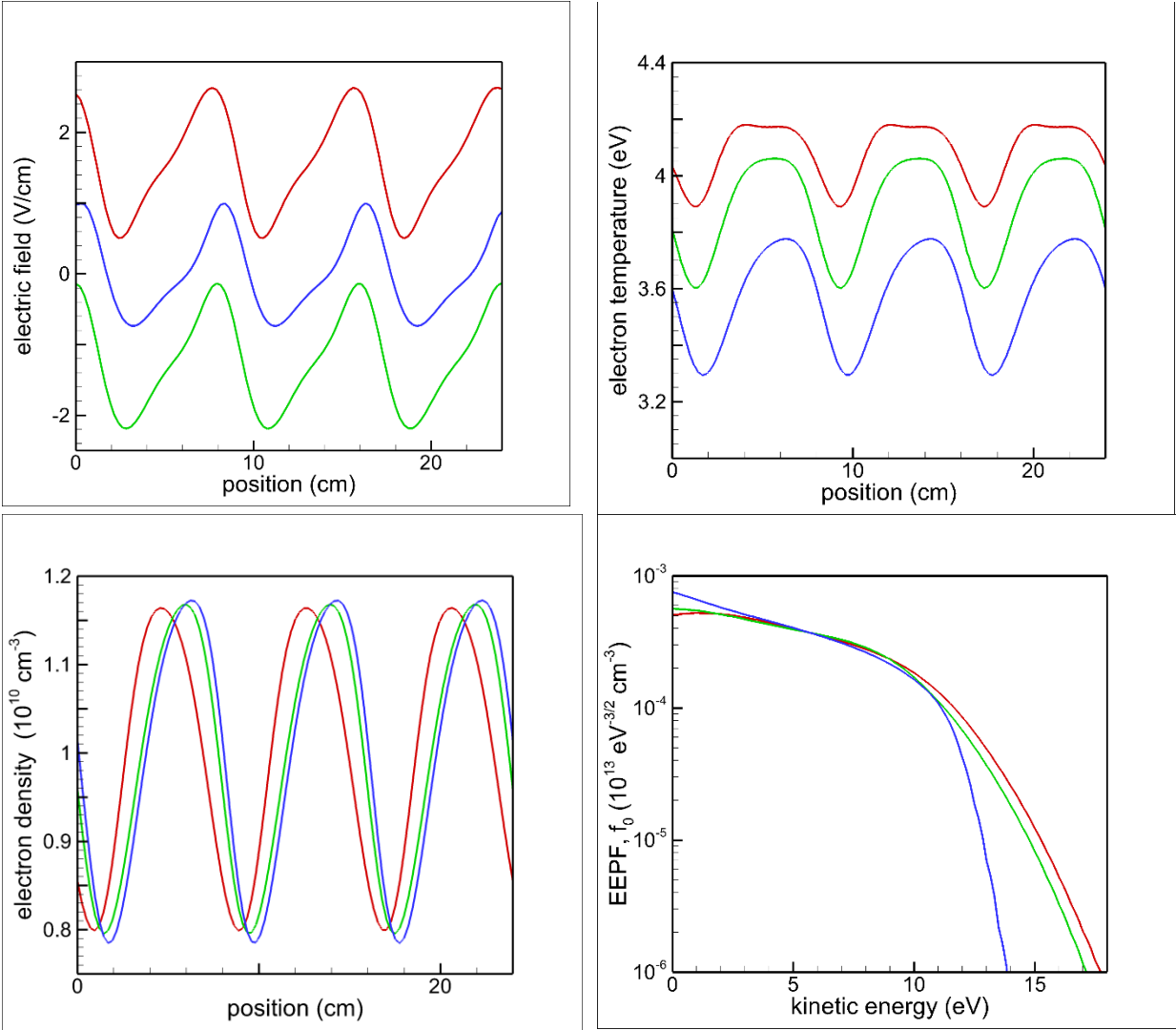


Figure 4: Instantaneous spatial distributions of the electric field (a), electron temperature (b), and electron and ion densities (c) and EEDF at  $x = 4$  cm three times during the AC period. Argon, 0.1 Torr, 0.1 MHz,  $E_0 = 1.86$  V/cm.

Figure 5 shows results for the driving frequency of 50 MHz and voltage  $U = 45$  V. The column length is  $L = 6$  cm, and the amplitude of the electric field is  $E_0 = 7.5$  V/cm. Under these conditions, plasma is strictly quasineutral, as the calculated Debye length of 0.3 mm is much smaller than the tube radius  $R = 0.52$  cm. Three standing striations are formed with a length of  $\Lambda = 2$  cm. The density of electrons does not change over the AC period, but oscillations of the electron temperature around their average value are still present.

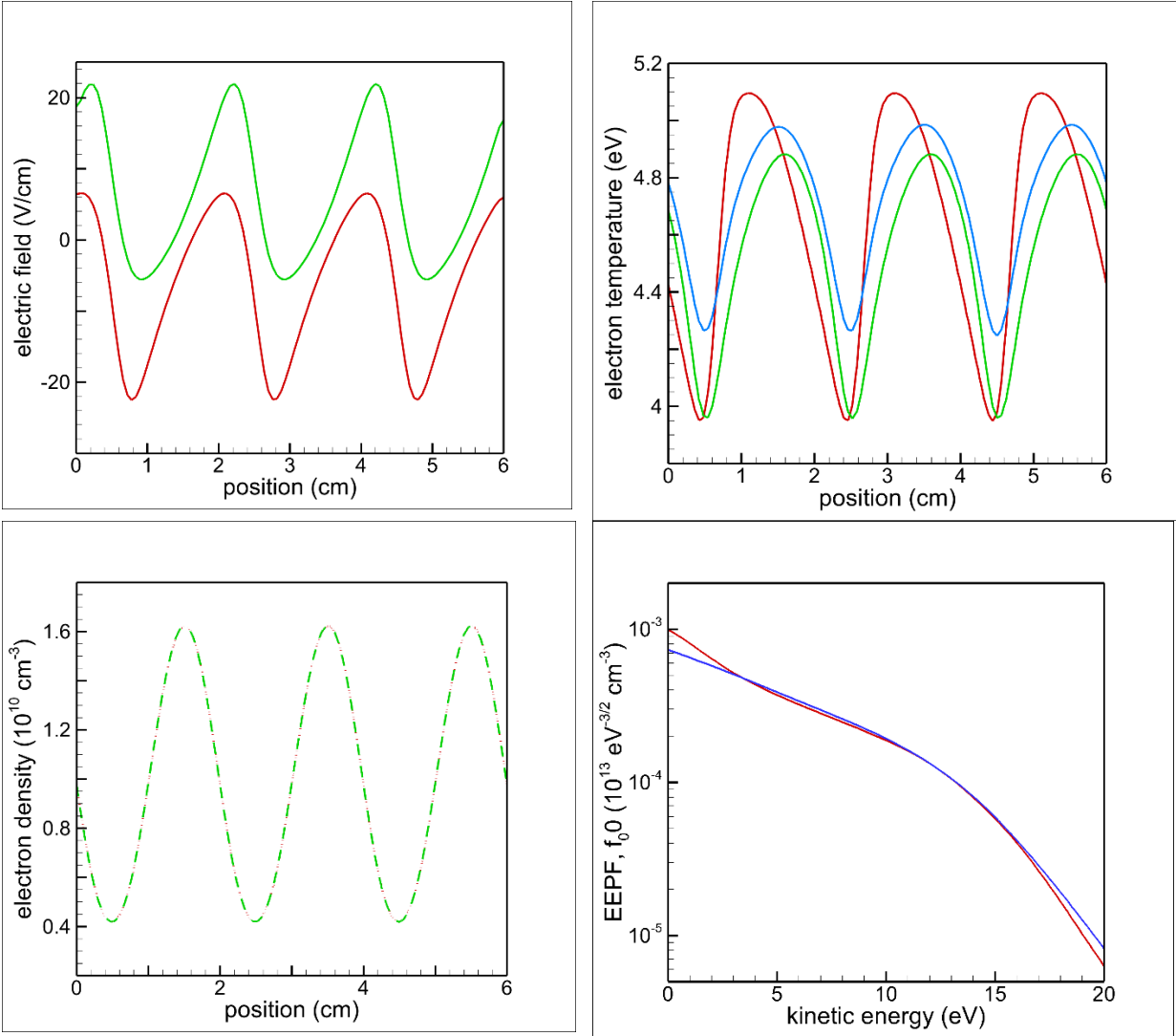


Figure 5: Instantaneous spatial distributions of the electric field, electron temperature, electron density, and EEDF at a point  $x = 2$  cm. Argon, 0.1 Torr, 50 MHz,  $E_0 = 7.5$  V/cm.

The oscillations of electron temperature are associated with substantial oscillations of the low energy part of the EEDF, which is responsible for the heat transport processes. The oscillations of the EEDF tail result in temporal variation of excitation and ionization rates. The heat transport occurs at the rate of free electron diffusion, which is much faster than the ambipolar diffusion controlling the plasma density profile. This explains why the temporal variations of electron temperature in spatially non-uniform plasma are observed even for such high driving frequencies.

Figure 8 compares temporal variations of the electric field, electron temperature, and electron densities in the middle of the column for 0.1 and 50 MHz. At 0.1 MHz, substantial oscillations of the plasma density are observed, whereas the density oscillations at 50 MHz are negligible. The temperature oscillations at 0.1 MHz occur at double the driving frequency, whereas at 50 MHz, they occur at the driving frequency. The difference in the absolute values of the electric field at the given point is due to the different positions for the spatial density maximum of the striation.

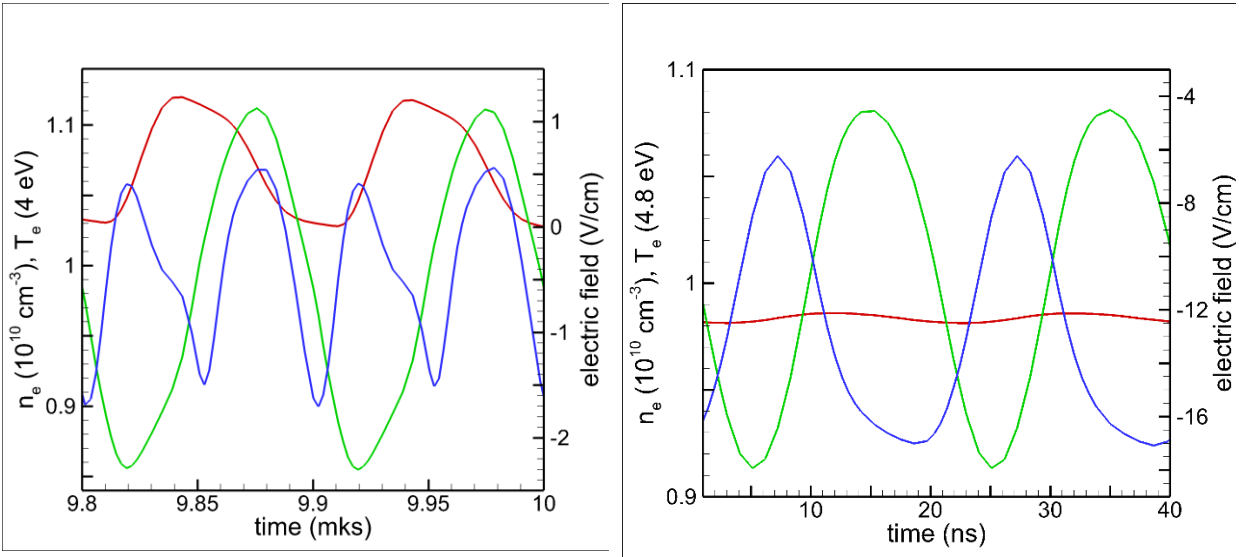
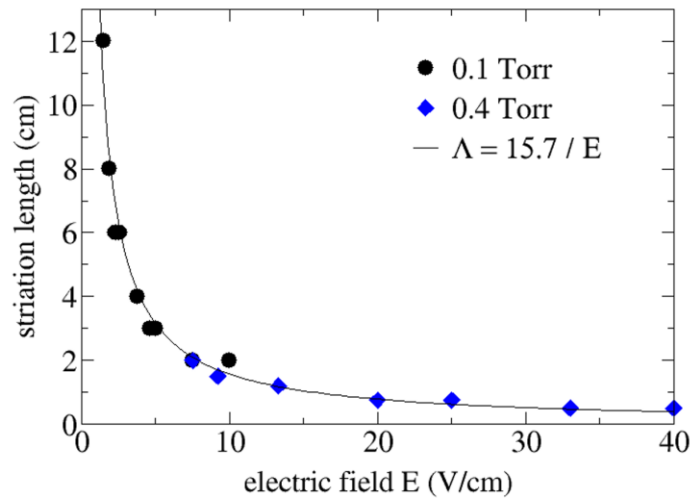


Figure 6: Temporal variations of the electric field (green), electron temperature (blue), and electron densities (red) at  $L/2$  for 0.1 MHz (left) and 50 MHz (right) in Argon at  $p = 0.1$  Torr.

Figure 7 summarizes the dependence of striation length on the electric field amplitude and tube radius observed in our simulations. For a wide range of electric fields, the  $\Lambda(E)$  dependence fits well by the formula,  $\Lambda = a/E$ , where  $a = 15.7$  eV. According to Novak's law, the expected value of  $a$  should be between the excitation and ionization thresholds, which are  $\varepsilon_1 = 11.55$  and  $\varepsilon_i = 15.8$  eV for Argon. Therefore, the observed dependence of the striation length on the electric field in Argon AC discharges obeys Novak's law. It is seen in Figure 7 (b), the striation length is about a few tube radii, which generally agrees with experiments.



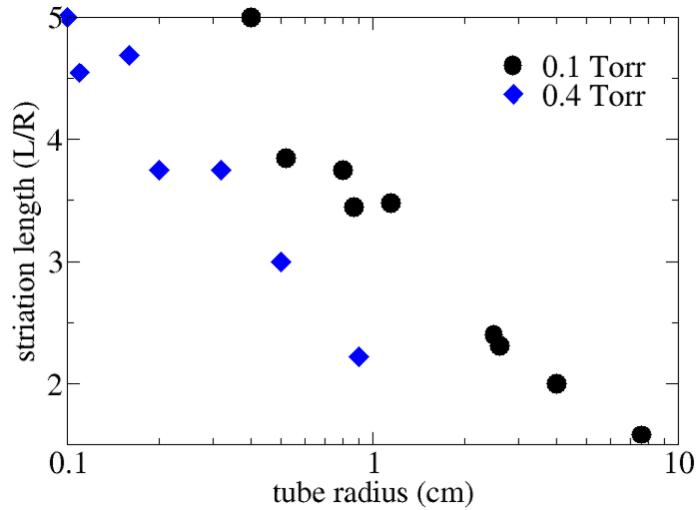
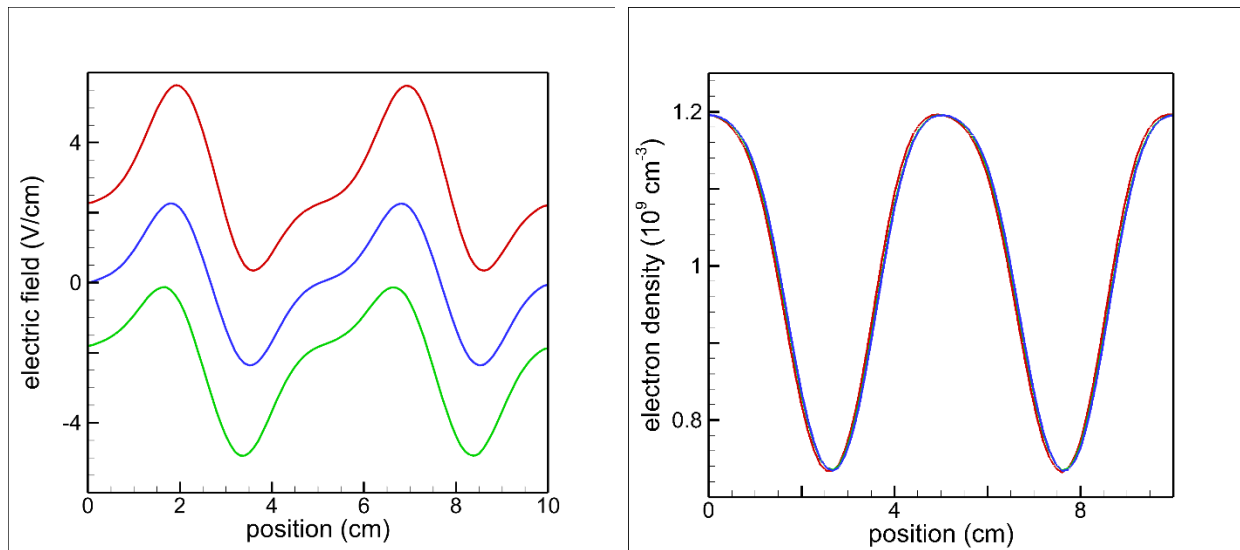


Figure 7: Striation length vs. the electric field (top) and tube radius (bottom) in Argon.

## 2. Standing Striations in Neon

Our simulations for Neon also produced standing striations at  $p = 1$  Torr, electric fields 3 - 15 V/cm, and driving frequencies of 0.1, 1, and 10 MHz. Figure 8 shows results for 1 MHz, and  $U = 30$  V. The column length  $L = 10$  cm corresponds to the electric field  $E_0 = 3$  V/cm. Our simulations observe two low amplitude striations with length  $\Lambda = 5$  cm for the tube radius  $R = 3.3$  cm. The ion and electron densities are practically constant over the AC period, but substantial temporal oscillations of electron temperature, EEDF tail, and the associated ionization rate occur.



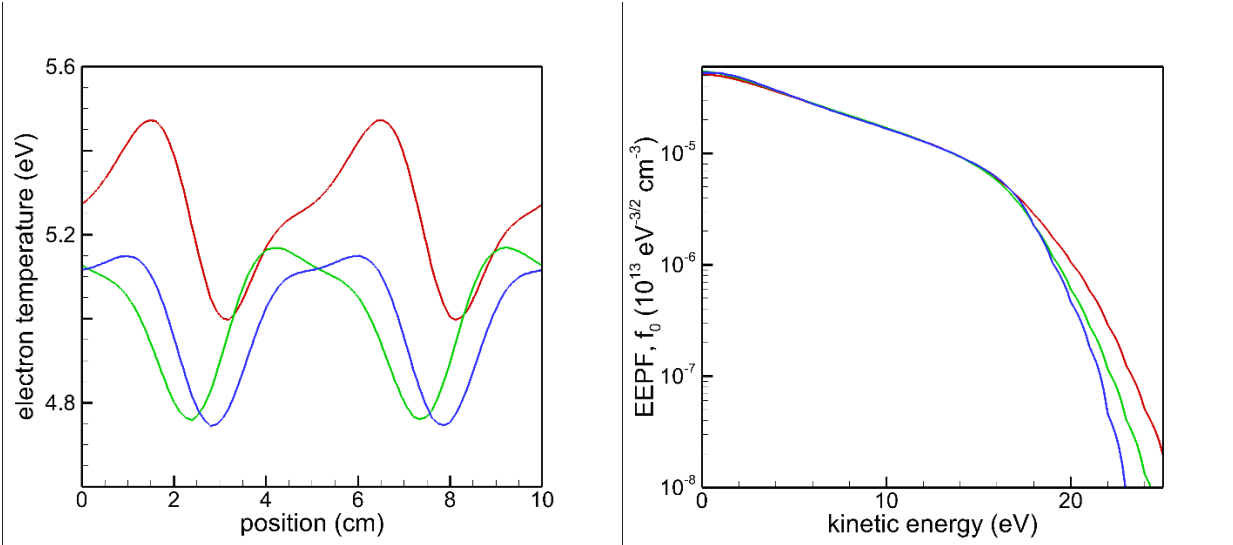
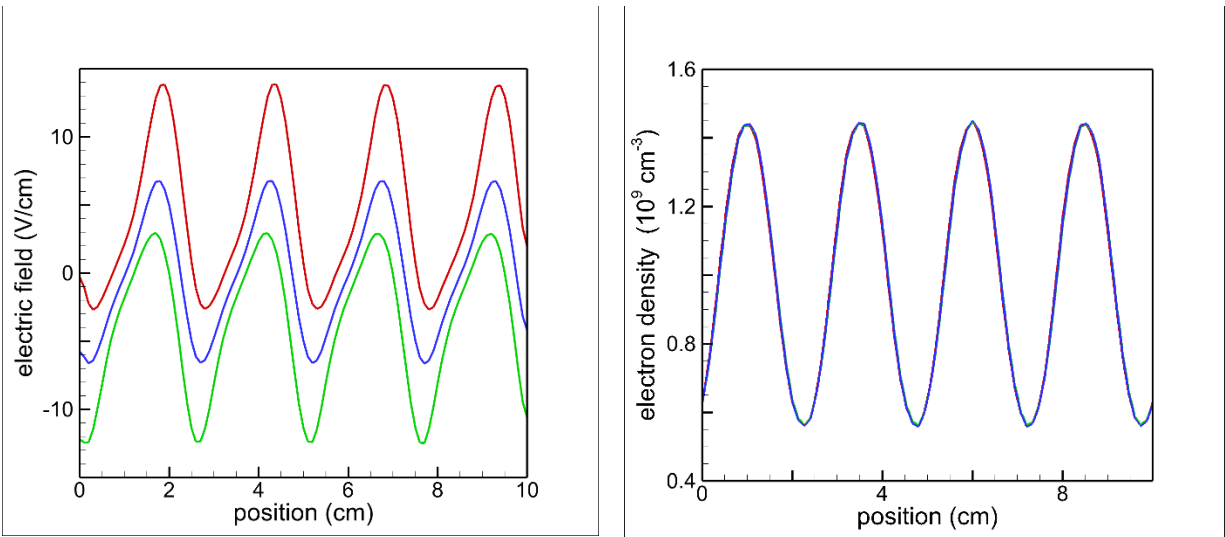


Figure 8: Time and space resolved electric field, electron density, electron temperature, and EEDF in Neon at 1 MHz,  $E_0 = 3$  V/cm.

Figure 9 shows results for 0.1 MHz,  $U = 50$ V. The electric field amplitude is  $E_0 = 5$  V/cm, calculated tube radius  $R = 1.6$  cm, and Debye length is 1 mm.



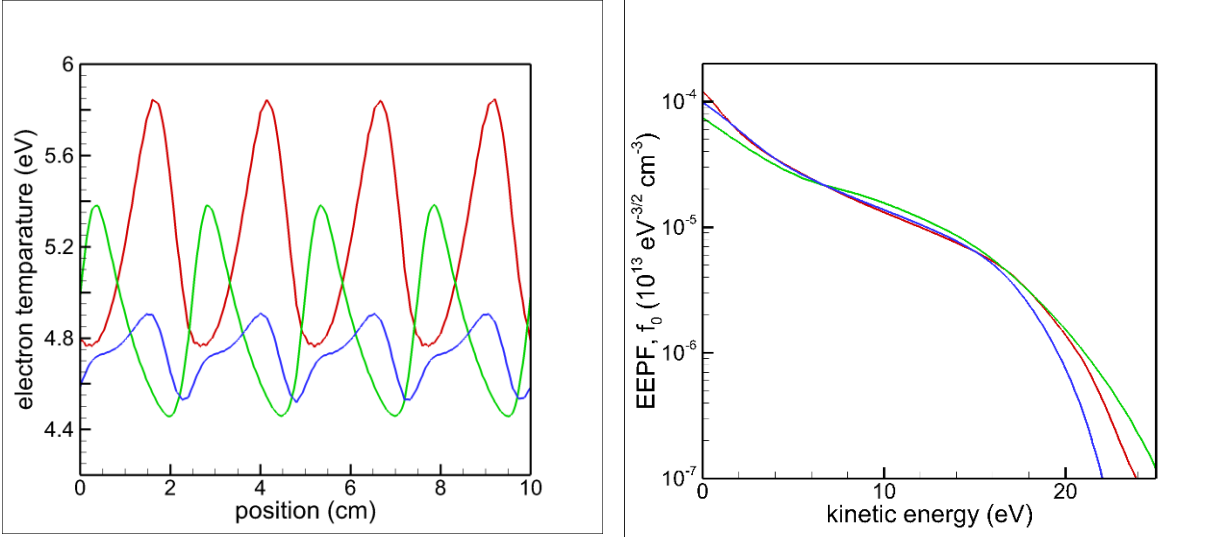


Figure 9: Time and space resolved electric field, electron densities, electron temperature, and EEDF at  $x = 3$  cm for Neon, 0.1 MHz,  $E_0 = 5$  V/cm.

Figure 10 compares temporal variations of the electric field, electron temperature, and electron densities in the middle of the column for 0.1 and 1 MHz. At 0.1 MHz, small oscillations of the plasma density are observed, whereas the density oscillations at 1 MHz are negligible. The temperature oscillations at 0.1 MHz are substantial and occur at double the driving frequency, whereas at 1 MHz, they are small and occur at the driving frequency. The absolute values of the electric field at the given point depend on the position of the point for plasma density maximum in the striation.

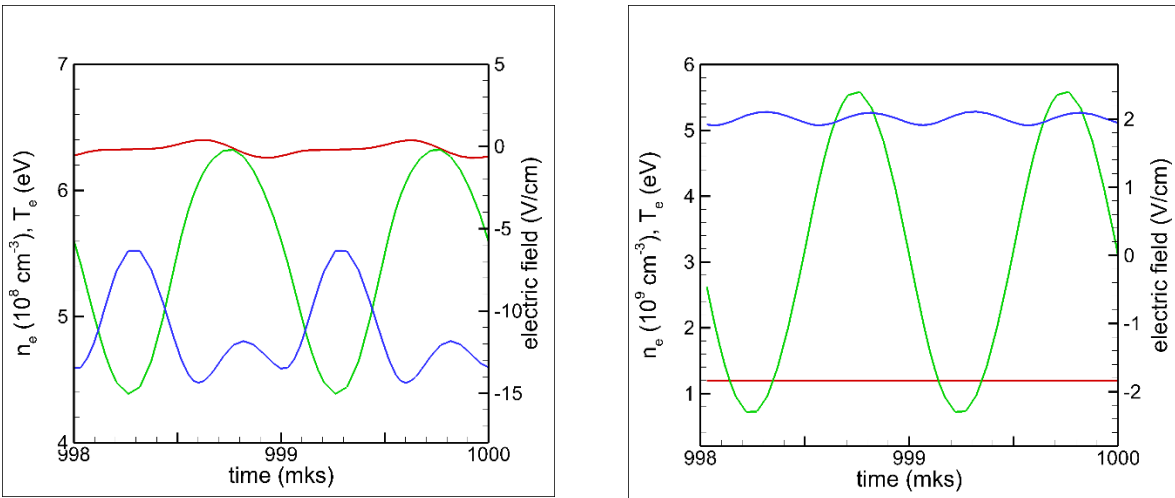


Figure 10: Temporal variations of the electric field (green), electron temperature (blue), and electron densities (red) at  $L/2$  for 0.1 MHz (left) and 1 MHz (right) in Neon at  $p = 1$  Torr.

Figure 11 summarizes the dependence of striation length on the electric field and tube radius observed in our simulations for Neon. The  $\Lambda(E)$  dependence fits the formula,  $\Lambda = a/E$ , with  $a = 16$  eV. According to Novak's law,  $a$ 's expected value should be between the excitation and ionization thresholds, which are  $\epsilon_1 = 16.62$  and  $\epsilon_i = 21.6$  eV for Neon. The  $\Lambda(E)$  dependence looks

good; however,  $a$ 's value is slightly lower than expected. The overall agreement appears satisfactory, considering a simplified two-level Neon atom and simple plasma chemistry. The striation length is about the tube radius, which agrees with experiments.

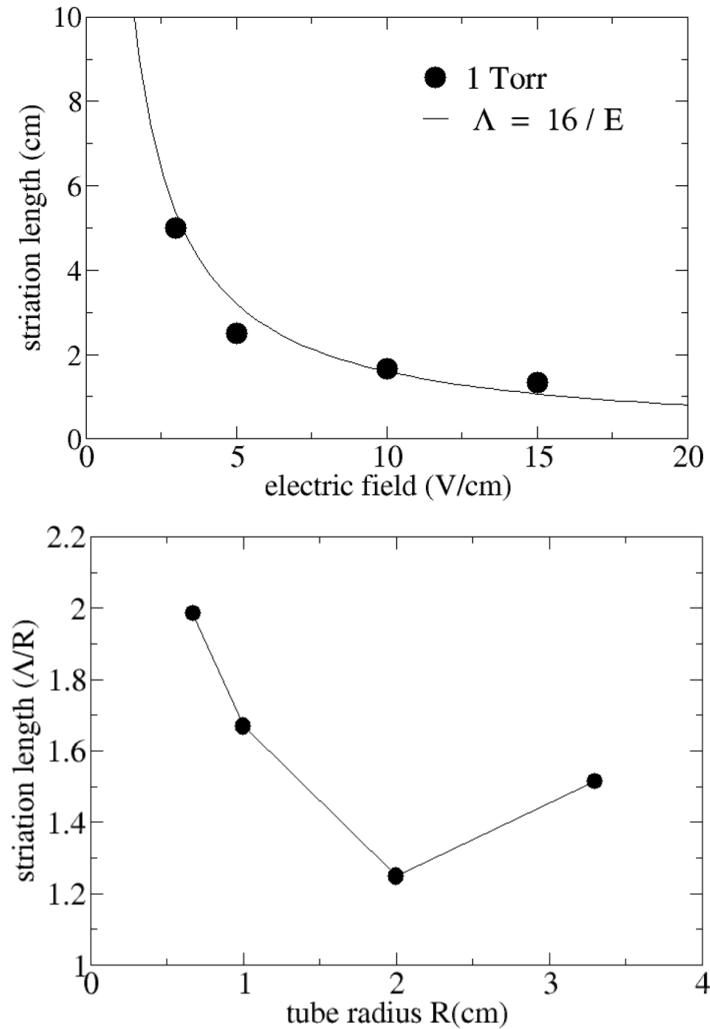


Figure 11: Striation length vs. the electric field (top) and tube radius (bottom) in Neon.

### 3. Mechanism of plasma stratification in AC positive column

Our simulations described above demonstrate that the electric field in AC discharge plasma can be separated into ambipolar and conduction components,  $\mathbf{E}(\mathbf{r}, t) = \mathbf{E}_a(\mathbf{r}, t) + \mathbf{E}_c(\mathbf{r}, t)$ , which evolve at different time scales. The ambipolar field is controlled by slow ion motion and evolves at the slow (ambipolar diffusion) time scale. This field can be written as  $\mathbf{E}_a = -\nabla\varphi$ , where  $\varphi(\mathbf{r}, t)$  is the electrostatic potential [23]. The conduction component evolves at the time scale associated with driving frequency  $\omega$ . The conduction electric field,  $\mathbf{E}_c(\mathbf{r}, t)$  describes electric current in plasma and electron heating.

In this section, we calculate the electric field in plasma from the current conservation [17]:

$$E(x, t) = \frac{j(t)}{eb_en_e(x)} - \frac{T_e(x, t)}{en_e} \frac{\partial n_e}{\partial x} = E_c(x, t) + E_a(x, t) \quad (26)$$

Here,  $E_c(x, t)$ , is a resistive component responsible for the conduction current and  $E_a(x, t)$  is the ambipolar field responsible for plasma quasineutrality. The field separation model has been previously used for simulations of the AC positive column where the axial (resistive) and radial (ambipolar) electric fields are orthogonal [21]. The field separation model is commonly used for ICP at high driving frequencies but has been rarely applied for CCP because it may not be applicable in the sheaths (see Section IV below).

We have seen in the previous section that in the range of driving frequencies,  $\omega\langle\tau_a\rangle > 1$ , the ambipolar field oscillates slightly over time because the plasma density remains quasi-steady. The time oscillations of the ambipolar electric field at frequencies  $1/\langle\tau_a\rangle < \omega < \nu_u$  occur mainly because of electron temperature variations rather than density variations (this regime was labeled the dynamic regime).

$$E_a(x, t) = -\frac{T_e(x, t)}{en_e} \frac{\partial n}{\partial x} \quad (27)$$

The expression (27) for the resistive component neglects the temporal dispersion of plasma conductivity, which is appropriate for  $\omega \ll \nu$ . The latter can be easily included [11] and has been commonly used for ICP simulations [24].

In our simulation described in this section, the ambipolar field,  $E_a(x)$ , was computed by solving the Poisson equation with fixed zero potential at both ends of the column. The  $E_c(x, t)$  was computed from Eq. (26) by specifying the discharge current  $j(t)$  and neglecting the time variations of  $n_e$ , which is valid at  $\omega\langle\tau_a\rangle > 1$ :

$$E_c(x, t) = \frac{j(t)}{eb_en_e(x)}$$

This field separation model makes the analysis of electron kinetics in AC plasma more transparent. Using total energy  $\varepsilon = u - \varphi(x, t)$  as an independent variable, the kinetic equation (9) can be rewritten as:

$$\frac{\partial f_0}{\partial t} - \frac{\partial}{\partial x} \left( D_r \frac{\partial f_0}{\partial x} \right)_\varepsilon = \frac{1}{\sqrt{\varepsilon}} \frac{\partial}{\partial \varepsilon} \left( \sqrt{\varepsilon} D_u(x, t) \frac{\partial f_0}{\partial \varepsilon} \right) + S_0 \quad (28)$$

The left part of Eq. (25) describes electron diffusion in phase space  $(x, u)$  over surfaces of constant total energy  $\varepsilon = u - \varphi(x, t)$ . The field  $E_c(x, t)$  contributes to electron heating, which is proportional to  $E_c^2(x, t)$ .

We assume that the conduction current,  $j(t) = j_0 \cos(\omega t)$ , and the electric field  $E_c(x, t) = E_0(x) \cos(\omega t)$  are monoharmonic. By taking the integral (4), we obtain [28]:

$$D_u(x, t) = D_0 \frac{1}{2} \left\{ (1 + \cos(2\omega t)) \left( \frac{v^2}{\omega^2 + v^2} \right) + \sin(2\omega t) \left( \frac{v\omega}{\omega^2 + v^2} \right) \right\} \quad (29)$$

where  $D_0(x) = E_0^2(x) D_r$ . At  $\omega \ll v$ , this formula corresponds to a quasi-static case:

$$D_u(x, t) = D_0 \cos^2(2\omega t) \quad (30)$$

At  $\omega \gg \nu_u(u)$ , the EEDF  $f_0(\mathbf{r}, u, t)$  is controlled by the time average field:

$$D_u(x, t) = D_0 \frac{1}{2} \frac{v^2}{v^2 + \omega^2} \quad (31)$$

In noble gases,  $\nu_u(u)$  is a strong function of electron kinetic energy, and the time scale for temporal EEDF relaxation in the elastic and inelastic energy ranges differs substantially.

Figure 12 shows results of simulations for a high driving frequency of 50 MHz at Argon pressure of 0.4 Torr when Eq. (28) is applicable, and  $j_0 = 20 \text{ mA/cm}^2$ . The calculated  $R = 3.7 \text{ mm}$ ,  $E_0 = 15 \text{ V/cm}$ , Debye length is 0.2 mm, and striations length is  $\Lambda = 1 \text{ cm}$ . The EEDF is enhanced by high-energy electrons at the points of maximal plasma density where the heating occurs.

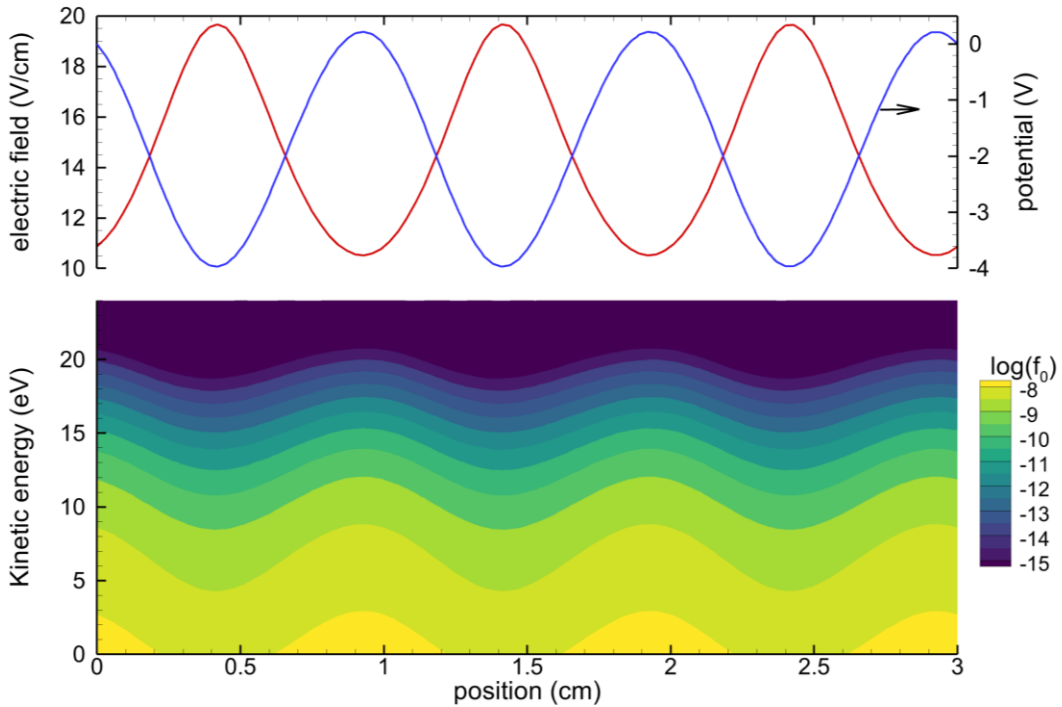
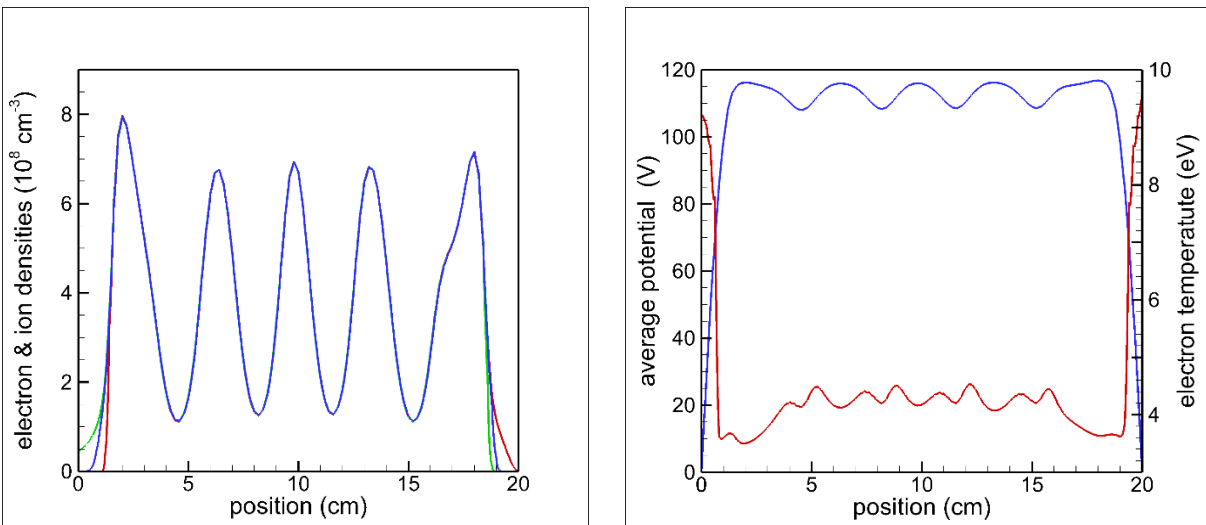


Figure 12: Spatial distributions of the ambipolar potential (blue), resistive electric field (red), and EEDF in Argon at 50 MHz, 0.4 Torr,  $j_0 = 20 \text{ mA/cm}^2$ .

The intrinsic spatial scale  $\lambda_\varepsilon = \varepsilon_1 / (e\langle E \rangle)$  determines the wavelength of striations, where  $\langle E \rangle = U/L$  for the DC case and  $\langle E \rangle = U/L/\sqrt{2}$  for the AC case.

#### IV. Effects of electrodes on plasma stratification

We have also performed simulations of CCP with resolved RF sheaths. The electron emission from electrodes was neglected, which corresponds to the  $\alpha$  mode of CCP operation. Figure 13 shows an example of simulations in Neon at  $p = 0.5$  Torr, an interelectrode gap of 20 cm, tube radius  $R = 1$  cm, driving voltage 300 V, and frequency of 3 MHz. Nonlinear standing striations with a wavelength of about 4 cm are formed inside the gap. Plasma density has maximum values at the minimum of the time-average electric potential. The depth of the potential well for electrons is lower by about 30 V than the amplitude of the applied voltage. The electron and ion densities respond to the time average electric field in the plasma; they do not change substantially over the RF period. Ions also respond to the time-average field inside the sheath, whereas electrons respond to the instantaneous field. The electron temperature oscillates substantially in time (and space) in plasma, corresponding to the dynamic discharge operation regime.



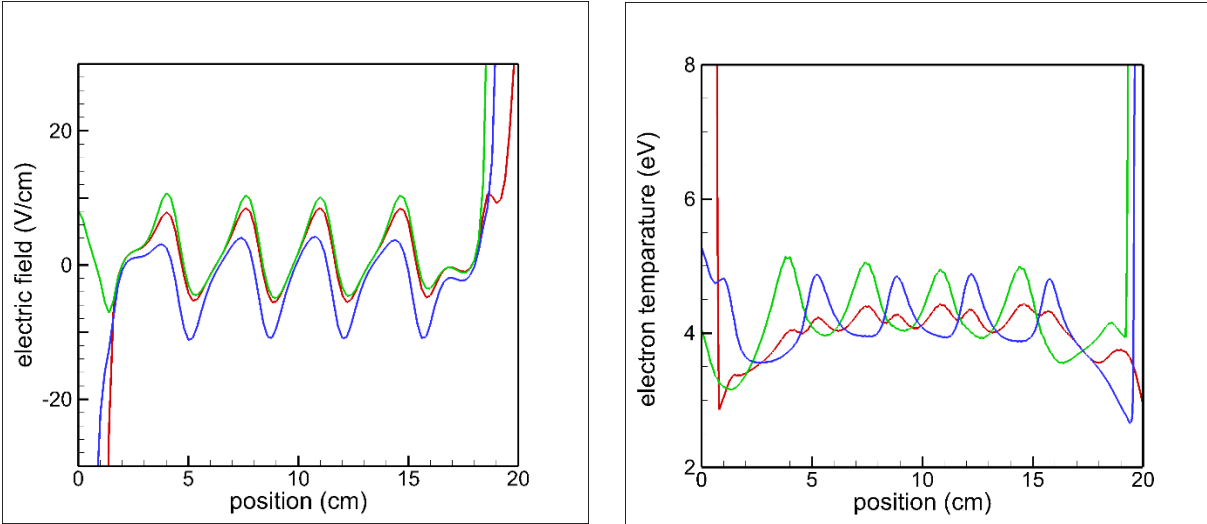


Figure 13: Instantaneous spatial distributions of electron and ion densities, period-average distributions of the electric potential and electron temperature, electric field, and electron temperature.

The main difference between the striations with periodic BCs is a non-sinusoidal time dependence of the electric field  $E(t)$  in the plasma due to the nonlinear processes in the RF sheath (Figure 14). The analysis of particle kinetics in the sheath and near-electrode effects is beyond the scope of the present paper. We have observed in our simulations that any asymmetry of discharge induces a DC electric field and slow motion of striations, as was previously observed in experiments [17].

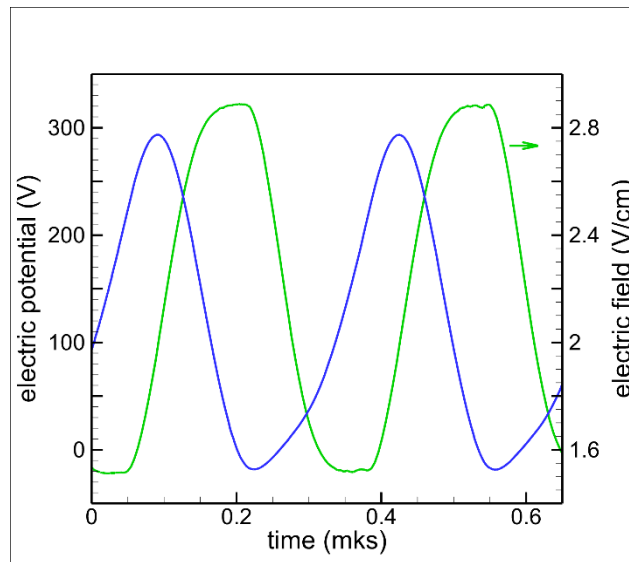


Figure 14: Time variations of the electric field and potential in the middle of the gap.

## V. Discussion

We conducted self-consistent simulations of standing striations in AC discharges of noble gases with a hybrid model accounting for nonlocal electron kinetics. The spatial non-locality of the EEDF is associated with two intrinsic spatial lengths:  $\lambda_\varepsilon = \varepsilon_1/(eE)$  over which the electrons gain kinetic energy equal to the excitation threshold of atoms  $\varepsilon_1$ , and  $\lambda_u = \lambda(\nu/\nu_u)^{1/2}$  the energy relaxation length for electrons in collisions. The minimum of these lengths defines striation length in stratified plasma. At  $\lambda_\varepsilon < \lambda_u$ , which corresponds to the inelastic energy balance of electrons, several types of striations with lengths close to integer fractions of  $\lambda_\varepsilon$  appear in DC discharges at low currents. In the opposite case,  $\lambda_\varepsilon > \lambda_u$ , which corresponds to the elastic energy balance of electrons, one type of wave with a length  $\Lambda \approx \lambda_u$  has been observed. We have shown that the kinetic model describes the experimentally observed standing striations in AC discharges at low currents, with the wavelength controlled by  $\lambda_\varepsilon$  under the studied conditions.

We found that electron heating occurs mainly at local maxima of plasma density and the ambipolar potential in stratified plasma conducting AC current. This distinguishes the stratified plasma column from the previously studied ICP, where the electron heating by the RF field occurs in the skin layer, and CCP, where the heating occurs in the sheaths near plasma boundaries [29]. The mechanism of stratification is related to the thermocurrent instability predicted by Timofeev [11] for wavelengths longer than the energy relaxation length of electrons in elastic collisions at  $\Lambda > \lambda_u$ . Timofeev used a reduced fluid model for electrons without an energy balance equation, which is justified when a non-Maxwellian EEDF is controlled by the local value of  $E/N$ . He considered both the DC and the high-frequency case,  $\omega \gg \delta\nu$ , and thus first predicted the thermocurrent instability as an origin of stratification for high-frequency discharges. Timofeev considered the conditions of the elastic energy balance of electrons and neglected inelastic collisions and ionization processes. The thermocurrent instability appeared when the thermodiffusion electron flux exceeded the diffusion flux. Shveigert [30] conducted numerical instability analysis for Helium DC discharges using the kinetic equation of electrons with account for inelastic collision and direct ionization by electron impact. He confirmed that the thermocurrent instability in Helium occurs at  $E/N = 4 - 7$  Td. Shveigert observed that switching off the ionization unsubstancially changes the instability increment at  $E/N < 7$  Td. Dyatko et al [31] conducted a kinetic study of the linear stage of thermocurrent instability in DC electric field and showed that the increment of this instability has a maximum at  $\Lambda \approx \lambda_u$ . They emphasize that the fluid description of electrons is invalid under these conditions without Coulomb interactions among electrons.

It is known that fluid models with the added energy balance equation for electrons can capture some nonlocal kinetic effects [32], [33]. Such models are well justified for noble gases at large plasma densities (currents) at  $\Lambda > \lambda(\nu/\nu_{ee})^{1/2}$ , where  $\nu_{ee}$  is the frequency of Coulomb collisions among electrons, and they have been successfully used in [18,17] for striations DC and RF discharges in noble gases. Fluid models with the energy balance equation for electrons can also be justified for molecular gases where excitations of the vibrational state of molecules shorten the energy relaxation length of electrons [34]. Recently, fluid models with the energy balance equation for electrons have been used to study plasma stratification in DC [13] and RF [4,7] discharges of noble gases. Unsurprisingly, such models can describe some features of stratification in noble gases by capturing some nonlocal effects. However, they fail to describe details, such as Novak's law and the kinetic resonances responsible for several types of striations in DC discharges in noble

gases at low currents observed in experiments. The kinetic model of electrons developed in [19] and used in the present paper is well suited to describe these phenomena. We have shown that the length of striations is about the radius of the tube and observed an analog of Novak's law for plasma stratification in AC discharges. However, we found only one striation (S wave) type in Argon and Neon plasma simulations described in the present paper. Can other resonances be observed in AC discharges?

We have used two models to calculate the electric field in the positive column. The first model solved the Poisson equation for an applied AC voltage between the column ends. The second model separated ambipolar and resistive components for a specified discharge current. In both models, the radius of the tube was calculated self-consistently for a given  $E/p$  to balance the particle production and loss. Finally, the entire CCP discharge with RF sheaths near electrodes and a stratified plasma column was simulated in a third model. In the latter case, the tube radius  $R$  was an input parameter, and the electric field in the stratified plasma column was calculated self-consistently for this value of  $R$ . The full discharge model, including electrodes, is applicable at low driving frequencies and could be used in future work to analyze stratification in dielectric barrier discharges, which often operate in quasi-static regimes.

We have clarified the nature of plasma stratification in AC discharges of noble gases. According to the kinetic model, standing striations in symmetric AC discharges appear due to enhanced electron heating in the areas of large plasma density. The primary reason for this instability is the dependence of the heating rate on the square of the electric field. The heating does not depend on the field direction, unlike acceleration. We have illustrated that heat transport occurs at the rate of free electron diffusion, and the electron temperature oscillates substantially in the dynamic discharge regimes. We have shown that electron-impact ionization plays an important role in plasma stratification in addition to electron heat transport. In our simulations, striations did not form with the switched-off generation of electron-ion pairs in the ionization term (Eq. (13)). Switching off the particle generation gradually increased the tube radius  $R$  and striation length in our simulations. This confirms that standing striations are indeed ionization waves, not heat waves. Thermocurrent instability without ionization processes did not lead to plasma stratification in our simulations for noble gases.

We have identified three characteristic time scales controlling plasma stratification and discharge dynamics. The fastest is the collision time  $\tau$  and the associated momentum transfer frequency,  $\nu(u)$ , which control the EDF isotropization rate. The slowest time scale is the time scale  $\tau_a$  of the ambipolar diffusion to the wall. The third (intermediate) time scale,  $\tau_u$  and the associated frequency  $\nu_u$  correspond to the electron energy relaxation rate. In our simulations, standing striations in Argon and Neon appeared at  $\omega\langle\tau_a\rangle > 1$ . We have distinguished the high-frequency and dynamic regimes. In the high-frequency case,  $\omega\tau_u > 1$ , the EEDF responds to the time-averaged AC electric field. In the dynamic regime,  $\nu_a < \omega < \nu_u$ , the EEDF shape, electron temperature, and ionization rate oscillate substantially over the AC period. The dynamic regime appears to be most efficient for plasma production as minimal power is required to sustain the plasma [15]. The low-frequency case,  $\omega < \tau_a$ , deserves separate studies. In this case, moving

striations formed at the fast electron time scale could be expected for a certain range of  $E/p$  and  $pR$ .

We have studied the range of  $E/N$  where the two-terms SHE and the FP kinetic equation for EEDF can be used. These are conditions when the electron mean free path  $\lambda$  is smaller than the tube radius  $R$ . In the case of  $\lambda > R$ , a solution to the full Boltzmann equation is required, which can be obtained using PIC or grid-based methods. This could be an interesting area for future research.

## VI. Conclusions

We have simulated standing striations in Argon and Neon AC discharges at driving frequencies exceeding the ambipolar diffusion frequency,  $\omega\langle\tau_a\rangle > 1$ . The numerical solution of a 2D kinetic equation for electrons in  $(x, u)$  phase space ( $u$  is kinetic energy) was coupled to the drift-diffusion model for ions and the Poisson solver for the electric field. We used a 2-level excitation-ionization model of noble gas plasma at low plasma densities, neglecting nonlinear effects caused by gas heating, stepwise ionization, and Coulomb interactions among electrons. Periodic boundary conditions have been applied to simulate standing striations in a positive column and clarify the nature of stratification.

We have shown that standing striations in symmetric AC discharges resemble moving striations in DC discharges under similar conditions. An analog of Novak's law was observed in our simulations for standing striations in Argon and Neon. Analysis of nonlocal electron kinetics in phase space demonstrated enhanced electron heating by the resistive electric field in the regions of high plasma density, with maximum excitation and ionization rates at these points. The primary reason for this effect and the associated plasma instability is the heating dependence of the square of the electric field. Electron heating does not depend on the field direction, unlike acceleration. Furthermore, we have shown that electron-impact ionization plays an important role in plasma stratification. Striations did not form in our simulations with the turned-off generation of electron-ion pairs. This confirms that standing striations are ionization waves, not heat waves. Thermocurrent instability without ionization processes did not lead to plasma stratification in our simulations for noble gases.

Although our model describes some experimental observations, further development is needed for quantitative comparison with experiments. We plan to include metastable atoms, stepwise ionization, and Coulomb collisions to study the effects of plasma density (discharge current) on striation properties. An important fundamental question is whether kinetic resonances responsible for several types of moving striations in DC discharges be observed in AC discharges in noble gases. The present work forms a solid foundation for the kinetic analysis of plasma stratification in molecular gases.

## Acknowledgments

This work was supported by NSF project OIA-2148653 and DOE project DE-SC0021391.

## References

---

- [1] V. I. Kolobov, Glow Discharges: Stratification, in *Encyclopedia of Plasma Technology*, Taylor & Francis (2017); Striations in rare gas plasmas, *J. Phys. D: Appl. Phys.* 39, R487 (2006)
- [2] A.V. Nedospasov, Striations, *Sov. Phys. Uspekhi* 11 (1968) 174.
- [3] A V Nedospasov and V D Haim, Fundamentals of the physics of processes in devices with low-temperature plasma, Moscow Energoatomizdat (1991) 224 p [in Russian]
- [4] V. Désangles, J.-L. Raimbault, A. Poyé, P. Chabert, and N. Plihon, Pattern Formation in Low-Pressure Radio-Frequency Plasmas due to a Transport Instability, *Phys. Rev. Lett.* 123, 265001 (2019)
- [5] Meng-Zhi Gu, Zhi-Cheng Lei, Xuan Zhang and Yi-Kang Pu, Transient striations in an inductively coupled plasma during E-to-H transitions, *2024 Plasma Sources Sci. Technol.* 33 025026
- [6] Meng-Zhi Gu, Zhi-Cheng Lei and Yi-Kang Pu, A two-region model for azimuthal striations in an inductively coupled plasma, *2024 Plasma Sources Sci. Technol.* 33 015007
- [7] D Levko and L L Raja, Influence of the Dufour effect on striations formation in radio-frequency discharges, *Phys. Plasmas* 31, 043504 (2024)
- [8] Y-X Liu, I Korolov, E Schüngel, Y-N Wang, Z Donkó and J Schulze, Striations in electronegative capacitively coupled radio-frequency plasmas: analysis of the pattern formation and the effect of the driving frequency, *Plasma Sources Sci. Technol.* 26 055024 (2017)
- [9] R Masheyeva, et al., Electron power absorption in CF<sub>4</sub> capacitively coupled RF plasmas operated in the striation mode, *Plasma Sources Sci. Technol.* 33 (2024) 045019
- [10] Y B Golubovskii, V O Nekuchaev, A Yu Skoblo, Advances in the study of striations in inert gases, *Technical Physics* 59 (2014) 1787
- [11] A V Timofeev, *Sov. Phys.—Tech. Phys.* 15 (1970) 140
- [12] N Dyatko et al., Non-thermal plasma instabilities induced by deformation of the electron energy distribution function, *Plasma Sources Sci. Technol.* 23 (2014) 043001
- [13] J P Boeuf, Ionization waves (striations) in a low-current plasma column revisited with kinetic and fluid models, *Phys. Plasmas* 29, 022105 (2022)
- [14] V I Kolobov, J A Guzman and R R Arslanbekov, A self-consistent hybrid model of kinetic striations in low-current argon discharges *2022 Plasma Sources Sci. Technol.* 31 035020

- 
- [15] V I Kolobov and Y B Golubovskii, The principle of minimal power, 2022 *Plasma Sources Sci. Technol.* 31 094003;
- [16] A. S. Penfold, J. A. Thornton, Structured Discharges in High Frequency Plasmas, *Czech. J. Phys. B* 23 (1973) 431
- [17] V I Kolobov, R R Arslanbekov, D Levko and V A Godyak, Plasma stratification in radio-frequency discharges in argon gas, *J. Phys. D: Appl. Phys.* 53 (2020) 25LT01
- [18] R R Arslanbekov and V I Kolobov, Advances in simulations of moving striations in DC discharges of noble gases, *Phys. Plasmas* 26, 104501 (2019)
- [19] V I. Kolobov and R R Arslanbekov, Ionization waves in low-current dc discharges in noble gases obtained with a hybrid kinetic-fluid mode, *Phys. Rev. E* 106, 065206 (2022)
- [20] V I Kolobov and V A Godyak, Inductively coupled plasmas at low driving frequencies, 2017 *Plasma Sources Sci. Technol.* 26 075013
- [21] N A Humphrey and V I Kolobov, Electron kinetics in a positive column of AC discharges in a dynamic regime, 2023 *Plasma Sources Sci. Technol.* 32 085017
- [22 ] C. Yuan, E. A. Bogdanov, S. I. Eliseev, and A. A. Kudryavtsev, 1D kinetic simulations of a short glow discharge in helium, *Physics of Plasmas* **24**, 073507 (2017)
- [23] A V Gurevich, *Nonlinear Phenomena in the Ionosphere*, Springer-Verlag New York Inc. (1978)
- [24] V.I. Kolobov and R.R. Arslanbekov, Simulation of electron kinetics in gas discharges, *IEEE Transactions on Plasma Science* 34 (2006) 895 – 909
- [25] W P Allis and S J Buschsbaum, in *Selected Works of William Phelps Allis* MIT Press (1967)
- [26] O. Michel, R. Duclous, P.-E. Masson-Laborde, C. Enaux, P. Lafitte, A nonlocal electron transport model in the diffusion scaling of hydrodynamics, *Physics of Plasmas* **30**, 022712 (2023)
- [27] D. W. Swain and S. C. Brown, Moving Striations in a Low-Pressure Argon Discharge, *Physics of Fluids* **14**, 1383 (1971)
- [28] V. E. Golant, A. P. Zhilinskii, and I. E. Sakharov, *Fundamentals of Plasma Physics*. New York: Wiley, 1980.

---

[29] V I Kolobov and V A Godyak, Electron kinetics in low-temperature plasmas, *Phys. Plasmas* 26, 060601 (2019)

[30] V A Shveigert, *Sov. J. Plasma Phys.* 14 (1988) 739

[31] N. A. Dyatko, I. V. Kochetov and A. P. Napartovich, Kinetic study of the linear stage of thermocurrent instability in the framework of the Boltzmann equation for a model gas, *Plasma Physics Reports* 37 (2011) 528

[32] J. H. Ingold, Nonequilibrium positive column, *Phys. Rev. E* 56 (1997) 5932

[33] L L. Alves, G Gousset, and S Vallée, Nonequilibrium Positive Column Revisited, *IEEE Trans. Plasma Sci.* 31 (2003) 572

[34] K Rohlena and H R Skullerud, Transport coefficients in a weakly ionized nonequilibrium plasma, *Phys. Rev. E* **51** (1995) 6028